Model-resolution based regularization improves near infrared diffuse optical tomography

Sree Harsha Katamreddy and Phaneendra K. Yalavarthy*

Supercomputer Education and Research Centre, Indian Institute of Science, Bangalore 560 012, India
**Corresponding author: phani@serc.iisc.in*

Received November 16, 2011; accepted January 17, 2012;
posted January 24, 2012 (Doc. ID 158123); published April 4, 2012

Diffuse optical tomographic imaging is known to be an ill-posed problem, and a penalty/regularization term is used in image reconstruction (inverse problem) to overcome this limitation. Two schemes that are prevalent are spatially varying (exponential) and constant (standard) regularizations/penalties. A scheme that is also spatially varying but uses the model information is introduced based on the model-resolution matrix. This scheme, along with exponential and standard regularization schemes, is evaluated objectively based on model-resolution and data-resolution matrices. This objective analysis showed that resolution characteristics are better for spatially varying penalties compared to standard regularization; and among spatially varying regularization schemes, the model-resolution based regularization fares well in providing improved data-resolution and model-resolution characteristics. The verification of the same is achieved by performing numerical experiments in reconstructing 1% noisy data involving simple two- and three-dimensional imaging domains. © 2012 Optical Society of America

OCIS codes: 170.0170, 170.0110, 170.3010, 170.6960, 100.3190.

1. INTRODUCTION

Functional imaging using diffuse optics has become attractive for soft-tissue imaging due to the non-ionizing nature of probing near infrared (NIR) light [1–4]. The NIR light having the wavelength range of 600–1000 nm is typically delivered using fiber optic bundles, which are placed on the surface (or boundary) of the tissue under investigation [2]. The diffuse light is collected also by the fiber bundles at the boundary, and the measured light intensities are used to obtain the optical absorption distribution [3]. When measurements from multiple wavelengths are available, these can lead to functional properties of the tissue, such as oxy-hemoglobin, deoxy-hemoglobin, and water concentrations [4].

The most important and critical step in diffuse optical tomography is estimating the internal distribution of absorption coefficient using the intensity-based boundary measurements, also known as the inverse problem [5–6]. The main aim of solving the inverse problem is to obtain estimates of optical absorption coefficient distribution by iteratively matching the experimentally measured data with the data obtained using a model (typically diffusion-based) [5]. This problem is nonlinear, ill-posed, and underdetermined, mainly due to dominance of scattering in NIR light propagation in tissue [6]. To overcome the ill-posedness of the inverse problem, i.e,. to obtain a unique solution for the inverse problem, a regularization is applied to the inverse problem [4–5]. The regularization (also known as penalty term) stabilizes the solution and primarily acts as a damping to overblown solution, either due to noise or instability of the inverse problem [5].

Several regularization schemes have been proposed in the literature that can effectively reconstruct the unknown absorption properties [7–14]. These could be broadly classified into two categories. The first one is based on the available prior information of the inverse problem. This prior information could be noise characteristics of the data or structural information obtained from other imaging modalities [7,14]. The more prior information one can use in the inverse problem, the better is the outcome of the reconstruction procedure and/or robustness to the noise in the data [7]. The second category is based on the physics of the problem. This could be as simple as using a spatially variant regularization or wavelength/chromophore specific regularization [10,15–16]. The simplicity associated with the physics based regularizations make them highly desirable for solving the inverse problem, especially in cases where the prior information is not available. Depending on the problem at hand and desired characteristics of optical image along with available prior information, the regularization is chosen to improve the quality and/or quantification of the reconstructed image. The spatially variant regularization captures the nonlinear variation of resolution characteristics of the problem and is also proven to improve the spatial resolution of the reconstructed optical image [10]. The penalty term in the spatially variant regularization comprises an exponential term, with higher value near the boundary and lesser penalty at the center of the imaging domain to counteract the hypersensitivity/bias close to the boundary, arising from detectors located on the boundary [10].

Here, the attempt will be to capture the non-uniformity in the resolution of the imaging domain using the model-resolution matrix and use the same as a penalty/regularization term to improve the spatial resolution in diffuse optical imaging. The model here refers to both sensitivity (Jacobian) and regularization term used to reconstruct the optical parameters. Usage of spatially invariant (or constant) regularization along with the sensitivity matrix leads to the model-resolution matrix, in turn giving the proposed regularization. Also, the use of model- and data-resolution characteristics for

 © 2012 Optical Society of America

the regularization/penalty schemes provided an objective way of assessing the performance of penalty terms. Using numerical experiments, it will be shown that the regularization based on the model-resolution matrix improves the spatial resolution and quantitative nature of the reconstructed optical images. As the emphasis of this work is on introducing and evaluating the new penalty term, the discussion is limited to a continuous-wave (CW) case, where the experimental measurement is the amplitude and the unknown optical parameter is the absorption coefficient.

2. MATERIALS AND METHODS

A. Continuous-Wave Diffuse Optical Imaging: Forward/Inverse Problem

The CW diffuse optical imaging of thick tissues, such as breast and brain, involves solving the steady-state diffusion equation (DE) given by [7,17]

$$-\nabla.\kappa(r)\nabla\Phi(r)+\mu_a(r)\Phi(r)=Q_o(r), \tag{1}$$

where $Q_o(r)$ is the isotropic CW source term located at position r and $\Phi(r)$ is the photon density (real-value). The absorption coefficient is represented by $\mu_a(r)$ and the diffusion coefficient by $\kappa(r)$, defined as

$$\kappa(r)=\frac{1}{3[\mu_a(r)+\mu_s'(r)]}, \tag{2}$$

with $\mu_s'(r)$ representing the reduced scattering coefficient. A Robin (type-III) boundary condition is employed to take care of the refractive-index mismatch at the tissue boundary [18]. A finite element based method is used to solve Eq. 1, which can handle irregular shaped imaging domains and provide stable solutions. The finite element framework is reviewed in [7,17]. The $\Phi(r)$ is sampled at the detector locations to give the amplitude data (A) and under the Rytov approximation the measured data are the natural logarithm of the amplitude ($\ln(A)$).

The inverse problem of diffuse optical imaging can be posed as a least-squares problem, where the aim is to iteratively match the experimentally measured boundary data with the modeled data. Because of the ill-posed nature of the inverse problem, a penalty term is always added to stabilize the solution [5]. The objective function with penalty term can be written as

$$\Omega=\|y-G(\mu_a)\|^2+P(\mu_a), \tag{3}$$

where y is the experimental data, i.e., $y=\ln(A)^{\text{measured}}$ and $G(\mu_a)$ is the modeled data. The penalty term is represented by $P(\mu_a)$, which stabilizes the solution and removes the high-frequency components. The objective function (Eq. 3) is minimized with respect to μ_a. Choice of $P(\mu_a)$ inadvertently affects the image quality, and there are many choices that have been proposed in the literature [7–14]. Here, the iterative procedure of minimizing Ω is stopped when $\|y-G(\mu_a)\|^2$ is not reduced by more than 2% between successive iterations, which ensures that experimental data match with modeled data within a small neighborhood. Two popular choices for the penalty term, based on the physics of the problem, are discussed in the following subsections.

B. Standard Penalty/Regularization Term

The standard penalty term here represents the Tikohnov type of regularization that is discussed in [13] with identity matrix as the regularization matrix, i.e.,

$$P(\mu_a)=\lambda\|\mu_a\|^2, \tag{4}$$

where λ is the regularization parameter that is constant and typically empirically chosen to stabilize the solution. The minimization scheme with this penalty term along with linearization leads to the updated equation (Gauss–Newton update equation) [13,19]

$$[J^TJ+\lambda I]\Delta\mu_a=J^T(y-G(\mu_a)), \tag{5}$$

where J is the Jacobian ($=\frac{\partial G(\mu_a)}{\partial\mu_a}$), which gives the rate of change of modeled data with respect to μ_a, dimension $\text{NM}\times\text{NN}$, where NM is the number of measurements and NN is the number of nodes (or imaging parameters) in the given mesh, and I represents the identity matrix. The transpose operation is indicated by T. The λ here is chosen as constant and plays an important role in terms of the resolution characteristics of the reconstructed image [7]. It will also be shown that the resolution provided by this penalty term tends to be more biased toward the detector location compared to other regularizations discussed in this work.

C. Exponential Penalty/Regularization Term

The exponentially varying regularization is similar to the earlier case, except that here it is spatially varying. That is,

$$P(\mu_a)=\lambda(r)\|\mu_a\|^2, \tag{6}$$

where $\lambda(r)$ is the spatially varying regularization parameter with r representing the spatial position. The spatial variation is achieved by exponential function that has the form (as discussed in [10])

$$\lambda(r)=\lambda_e\exp\left(\frac{r}{R}\right)+\lambda_c, \tag{7}$$

where R is the radius of the imaging domain, with λ_c and λ_e representing the regularization parameters that represents the center and edge location. These are chosen empirically as discussed in [10]. Similar to Eq. 5, the update equation here becomes

$$[J^TJ+\lambda(r)I]\Delta\mu_a=J^T(y-G(\mu_a)). \tag{8}$$

This form of the regularization captures the diagonal of the Hessian matrix (J^TJ) and has been shown to perturb the solution less than the constant penalty term [10]. This physics based regularization will also be shown to provide better resolution characteristics compared to the standard regularization term.

D. Model-Resolution Based Penalty/Regularization Term

The model-resolution matrix derivation involves the linearization of the problem. As the main aim of the optimization is to match experimental data with the model data, i.e., assuming $y=G(\mu_a)$, we can expand the $G(\mu_a)$ using Taylor series around μ_{a0}, giving

$$y = G(\mu_a) = G(\mu_{a0}) + G'(\mu_a)(\mu_a - \mu_{a0}) + (\mu_a - \mu_{a0})^T G''(\mu_a)(\mu_a - \mu_{a0}) + \ldots, \quad (9)$$

where $G'(\mu_a) = J$ and $G''(\mu_a)$ is the Hessian. Linearizing the above equation (ignoring all higher order terms) leads to

$$y = G(\mu_{a0}) + J(\mu_a - \mu_{a0}) \quad (10)$$

using $y - G(\mu_{a0}) = \delta$ (also known as data-model misfit) and $\tilde{\Delta\mu_a} = \mu_a - \mu_{a0}$. Representing the true update in μ_a gives

$$\delta = J\tilde{\Delta\mu_a}. \quad (11)$$

Substituting Eq. 11 in Eq. 5 (assuming $y - G(\mu_a) = \delta$) results in

$$\Delta\mu_a = [J^T J + \lambda I]^{-1} J^T J \tilde{\Delta\mu_a}. \quad (12)$$

The $\Delta\mu_a$ here represents the estimate of $\tilde{\Delta\mu_a}$. It could be noted that in the case of $\lambda = 0$, the estimated updated optical properties is equal to the true update, i.e., $\Delta\mu_a = \tilde{\Delta\mu_a}$. Because of the ill-posed nature of the problem, $\lambda > 0$, which also means $\Delta\mu_a \neq \tilde{\Delta\mu_a}$. This leads to the definition of the model-resolution matrix, which is given by

$$M = [J^T J + \lambda I]^{-1} J^T J, \quad (13)$$

which has the dimension of NN × NN and depends purely on the numerical characteristics of $J^T J$ and the regularization used (here it is λI). The estimated imaging parameters ($\Delta\mu_a$) are the weighted averages of the true imaging parameters ($\tilde{\Delta\mu_a}$), where rows of M provide the weights [20]. In the case $M = I$, the imaging parameters are exactly determined [20]. Also, the model-resolution matrix does not depend on the data (or the noise in the data). It is purely based on the forward problem and the regularization used. Note that the M is different for the standard and exponential penalty/regularization terms. In the case of exponential penalty, the model-resolution matrix is given by

$$M_r = [J^T J + \lambda(r) I]^{-1} J^T J, \quad (14)$$

where the suffix r for M denotes the spatially varying nature of the regularization used. The diagonal entries of the model-resolution matrix capture the nonlinear nature of the model, and the closer it is to unity, the better is the achieved resolution. This leads us to the definition of regularization based on model resolution, which is also spatially varying (similar to Eq. 6) and is defined as

$$\lambda_i = \frac{M_{ii}}{\max(M_{ii})} \quad \text{for } i = 1, 2, \ldots, NN, \quad (15)$$

where M_{ii} is the diagonal entries of M (Eq. 13) and λ_i indicates the i^{th} entry of the spatially varying regularization. The max here represents the operation of finding the maximum value. The penalty term for this scheme will be

$$P(\mu_a) = c\lambda_i \|\mu_a\|^2, \quad (16)$$

where c is a constant that provides a weight for the penalty term (typically chosen as less than 1). This penalty leads to the updated equation

$$[J^T J + c\lambda_i I]\Delta\mu_a = J^T(y - G(\mu_a)). \quad (17)$$

The normalization operation in Eq. 15 make sure that the effect of λ is minimal in getting the values of λ_i (also shown later). Note that the model-resolution matrix for this penalty term becomes

$$M_i = [J^T J + c\lambda_i I]^{-1} J^T J. \quad (18)$$

The aim is to show that M_i structure is more close to identity matrix, implying the resolution characteristics are better. Also note that as $\lambda > 0$ in Eq. 13, the maximum value λ_i can take is 1 and minimum value is 0 [20].

E. Data-Resolution Matrix

The model-resolution matrix provides an estimate of the image characteristics. It is also important to study the effect of penalty on the data-resolution. The data-resolution matrix arises from studying how well the estimated $\Delta\mu_a$ fits with the observed data (here it is δ) by rewriting Eq. 11 as

$$\delta_p = J\Delta\mu_a, \quad (19)$$

where δ_p is the predicted data-model misfit and $\Delta\mu_a$ is the estimate update in μ_a. Substituting for the estimated $\Delta\mu_a$ using Eqs. (5), (8), and (17) will result in the data-resolution matrix. It has the form [20]

$$D = J[J^T J + \tilde{\lambda} I]^{-1} J^T, \quad (20)$$

where $\tilde{\lambda}$ represents the regularization schemes that were employed in this work, namely, standard, exponential, and model-resolution based penalty terms: λ, λ_r, and $c\lambda_i$, respectively. The data-resolution matrix has the dimension of NMXNM and is similar to M. The closer it is to the identity matrix, the lower the data prediction errors are. The range of values for the entries of D is [0,1]. The diagonal values of D also give the importance of the corresponding data point, as it indicates the weight associated with its own prediction [20]. The higher the magnitude of the diagonal entry of D, the more important is the data point [20]. As is also evident from Eq. (20), the data-resolution matrix is not a function of data but depends on the model (J and the penalty term), similar to model-resolution matrix.

F. Numerical Experiments

For objectively assessing the effect of using a model-resolution based penalty, circular (2D) and cylindrical (3D) imaging domains are considered. These imaging domain background optical properties were set to $\mu_a = 0.01$ mm^{-1}, $\mu_s' = 1$ mm^{-1} with uniform refractive index of 1.33. The circular imaging domain with a diameter of 86 mm is discretized by 20160 linear triangular elements corresponding to 10249 number of nodes (NN). A cylindrical domain with the same diameter and having a height of 100 mm is discretized by using 63810 linear tetrahedral elements corresponding to 12695 nodes (NN). In both 2D and 3D cases, 16 fibers were spaced equally and arranged in a circular fashion, where at a time one fiber acts as a source and the rest act as detectors, leading to 240 (16 × 15) measurements and implying $NM = 240$. The source is modeled as a Gaussian source with a full-width-half-maximum of 3 mm to mimic the experimental case [21] and placed at

one scattering distance inside the imaging domain. Both 2D and 3D finite element meshes were centered at origin and the ring of fibers are placed at the center of Z-coordinate ($Z = 0$) for the 3D case.

The absorption targets that were considered in this work are circular and cylindrical in shape for 2D and 3D imaging domains, respectively, and had optical properties $\mu_a = 0.02\ \text{mm}^{-1}$, $\mu_s' = 1\ \text{mm}^{-1}$. As mentioned earlier, as only amplitude data were used in the reconstruction, the μ_s' is assumed to be known. A pixel-basis having 2500 elements (50×50) is used as a reconstruction basis for 2D case and $30 \times 30 \times 30$ grid for the 3D case. As the emphasis was on proving improved resolution characteristics using the model-based penalty term, resolving two targets that are separated by a small distance is considered as the test object. The data noise level was kept at 1% to mimic the experimental case [21]. This noisy data (numerically generated), along with the initial guess of the background optical values, are used in the reconstruction procedure. In all cases here, the values $\lambda = 0.2$ for standard regularization, $\lambda_c = 0.04$ and $\lambda_e = 0.1$ for exponential regularization, and $c = 0.2$ for the model-resolution regularization were used in reconstructing absorption images.

All computations are carried out on a Apple Mac workstation with dual quad-core 2.26 GHz Intel Xeon processor with 24 GB memory. The computations used the open-source NIRFAST for finite element method based modeling of near infrared light propagation in the tissue [22].

3. RESULTS

The composition of model-resolution based regularization (Eq. 15) involves computing M using Eq. (13), which uses the constant penalty term (λ). The effect of λ for computing the λ_i is studied by varying λ, for which the J is computed using a 2D homogenous mesh with background optical properties as given in Section 2F. The λ is varied from 0.001 to 1000 (resulting in a factor of 10 between successive steps) and the λ_i is plotted in the Fig. 1. The figure shows that variation of λ on the normalized diagonal values of M or λ_i has little to no effect, and any constant regularization based model-resolution matrix will provide similar characteristics (evident in Fig. 1). Note that $\lambda = 1$ is used throughout this work for calculating M and in turn λ_i.

To understand the effect of different penalty terms discussed earlier in Subsections 2.B, 2.C, and 2.D, the diagonal of the model-resolution matrices (normalized) corresponding to these penalty terms are plotted (Fig. 2). The model-resolution matrix forms are given in Eqs. (13–14), and (18) for standard, exponential, and model-resolution based penalty terms. The normalized diagonal entries of the same for a uniform mesh (similar to earlier) is plotted in Fig. 2 as a function of radial distance. It is evident that variation in the model resolution is higher for the constant/standard regularization and the least being model-resolution based penalty term. Also note that at edge the resolution characteristics are similar for all penalty terms discussed here, but at the center the model-resolution based penalty provides better resolution characteristics, as the values are higher in magnitude and more close to 1.

As discussed in Subsection 2.E, the data-resolution matrix plays an important role in terms of predicted errors. This provides another quantitative way of analyzing the penalty terms, where the diagonal entries of D (Eq. 20) give the importance of data-points. The normalized diagonal entries of D using standard (constant), exponential, and model-resolution based penalty terms are plotted in Fig. 3. The model-resolution based penalty term provides higher magnitude of the diagonal entries of D, indicating that the importance to the corresponding data-points is higher in this case compared to other penalty terms. This also implies the prediction errors are lower for the case of model-resolution based regularization.

To assess the observations made based on model-resolution matrix characteristics, numerical experiments where two targets are located close to the center and vertically placed are considered. The radius of the targets is 7.5 mm and are separated by 5 mm (vertical distance). The target μ_a distribution is given in the top row first column of Fig. 4(a). The 1D cross-sectional value along Y-direction is plotted as a solid line in Fig. 4(b). The reconstructed absorption distributions obtained using the penalty terms discussed are given in the same figure (Fig. 4). Resolution of these

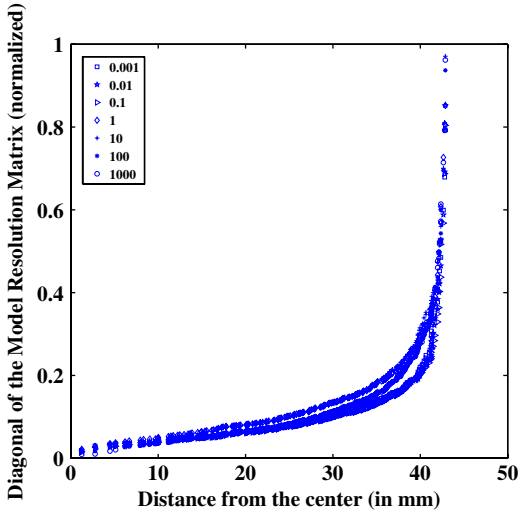

Fig. 1. (Color online) Plot of diagonal of model-resolution matrix (M, Eq. 13) versus spatial location in the imaging domain as a function of λ (values are given in the legend).

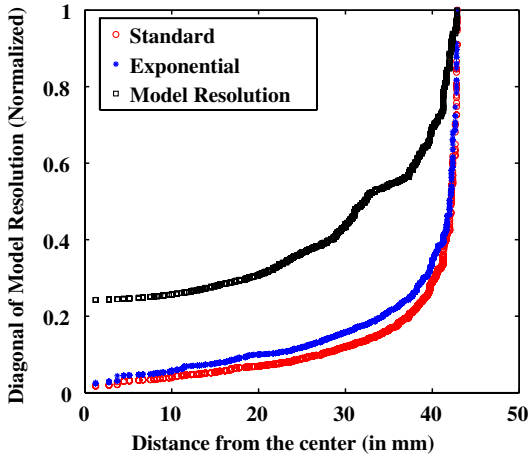

Fig. 2. (Color online) Plot of diagonal of model-resolution matrices for the regularization schemes versus the spatial location in the imaging domain. The model-resolution equation for standard regularization is given by Eq. 13, exponential by Eq. 14, and model-resolution one by Eq. 18.

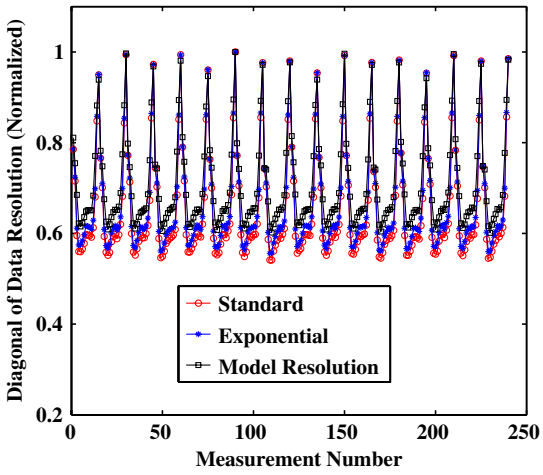

Fig. 3. (Color online) Plot of the diagonal of the data-resolution matrix (D, Eq. 20) for the regularization schemes used in this work versus the measurement number.

closely spaced targets is achieved using model-resolution based penalty term.

The sensitivity in diffuse optical imaging is known to be higher near the boundary [23]. Because of placement of source/detectors, the same effort of resolving two targets that are vertically separated and placed near to the boundary is taken up next. Same as above (Fig. 4), these have radius of 7.5 mm and are separated by 5 mm. The reconstruction results obtained using the regularization schemes discussed in this work are given in Fig. 5(a), along with the target distribution. The 1D cross-sectional plot along the vertical line passing through the centers of the targets ($x = 28.5$ mm) are given in Fig. 5(b). Even though standard and exponential penalty terms are able to resolve the targets, the regularization scheme that is based on the model-resolution matrix is more close to the target distribution.

A similar effort in 3D using cylindrical imaging domain is taken up to assess the effectiveness of model-resolution based regularization scheme and in here the targets are cylindrical ones (radius of 10 mm) extending in Z direction. These are placed close to the center of imaging domain (distance between the targets is 10 mm). The target 2D cross sections of the 3D volume in 9 mm increments from $z = -50$ mm to $z = 50$ mm from left to right are shown as top-row in Fig. 6(a). The reconstruction results are given in the rest of the rows in Fig. 6(a). A 1D plot obtained at $Z = 0$, across Y is given in Fig. 6(b) for the reconstruction results obtained in Fig. 6(a). The performance of exponential and model-resolution based regularization scheme is similar and better than the standard regularization. In case of same targets being placed close to the edge, reconstructed absorption distributions and cross-sectional plots are given in Fig. 7. The exponential penalty term performs better than the standard constant penalty, but the performance of model-resolution based scheme is within 5% of matching value obtained using exponential penalty. The typical number of iterations to reach the convergence was 18 for all three regularization schemes for both 2D and 3D cases presented in this work.

4. DISCUSSION

Diffuse optical tomographic imaging is known to be a ill-posed problem, which is compensated by a regularization/penalty term. The choice of the penalty terms dictates the solution of the problem. The prior information based regularization is known to provide more stabilized and accurate solution [9,13]. The regularization schemes based on the data, wavelength, and the parameter have also been proven to be more effective than the standard ones, with a caveat that they require information about the characteristics of the data (including noise level) [11,13,15,16]. In this work, a regularization scheme that is based on the model was introduced and shown to provide better spatial resolution characteristics compared to the ones existing in the literature. This regularization scheme does not require/assume any characteristics about the data and is purely based on the numerical-model that is used in obtaining optical images. Note that the exponential regularization scheme, which was based on the heuristics

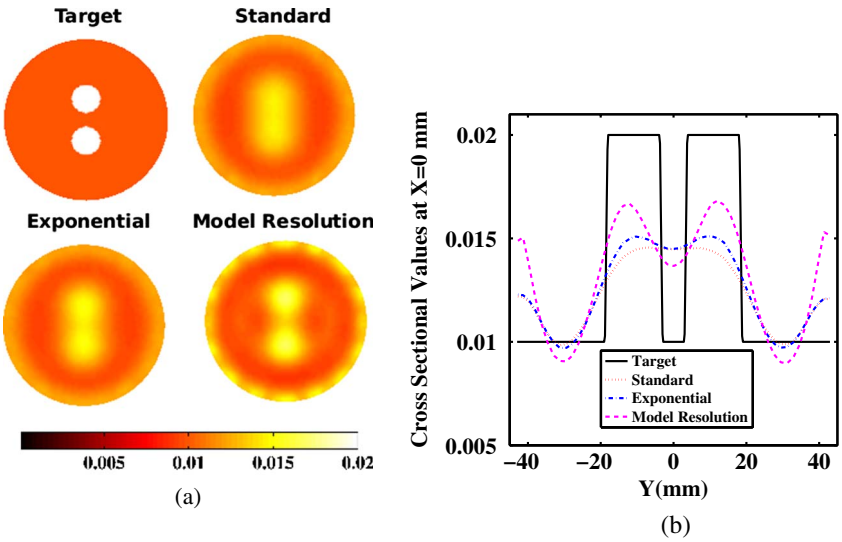

Fig. 4. (Color online) (a). Comparison of reconstruction performance in 2D using three regularization schemes discussed in this work for the circular targets located close to the center with numerically generated 1% noisy data. The reconstructed images obtained along with corresponding regularization scheme (given on top of image) are given along with the target image. (b). 1D cross-sectional plot of μ_a along the vertical line ($x = 0$ mm) for the target and reconstructed results presented in (a).

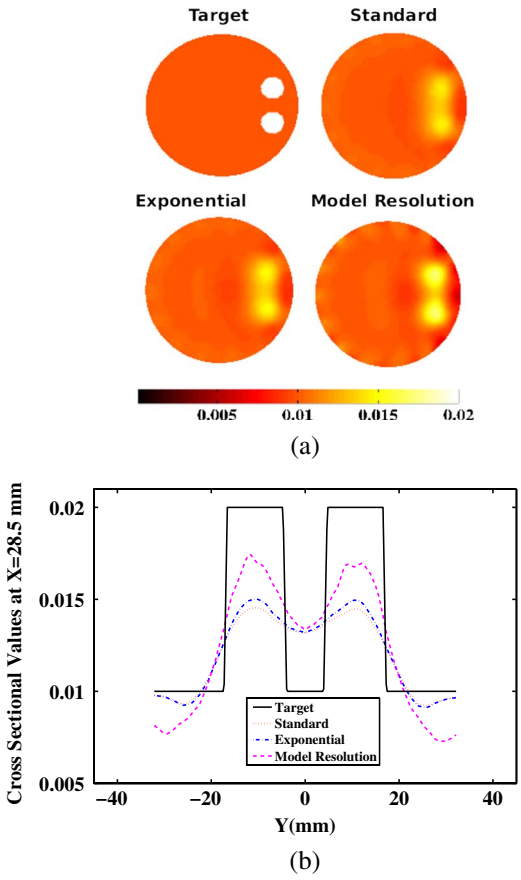

Fig. 5. (Color online) Similar effort to Fig. 4 except the targets are located close to the boundary (edge) of the imaging domain.

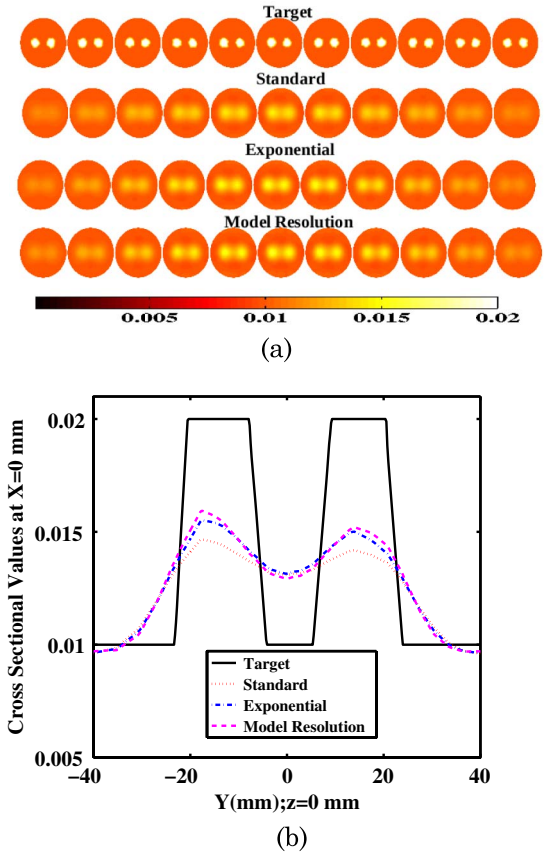

Fig. 6. (Color online) (a). Comparison of reconstruction performance in 3D using three regularization schemes discussed in this work for the cylindrical targets located close to the center with numerically generated 1% noisy data. 2D cross sections of the 3D cylindrical volume in 9 mm increments spanning from $z = -50$ mm to $z = 50$ mm from left to right are shown. The reconstructed distributions obtained along with corresponding regularization scheme (given on top of images) are given along with the target distribution. (b). 1D cross-sectional plot of μ_a at $Z = 0$ mm along the vertical line ($X = 0$ mm) for the target and reconstructed results presented in (a).

[10], was also used in this work and shown to be as effective as model-resolution based regularization in 3D [Fig. 6 and 7].

Obtaining λ_i in Eq. (15) requires construction of M (Eq. 13), which is one extra inversion ($O(NN^3)$) performed compared to other regularization scheme and any constant λ will lead to similar λ_i (Fig. 1). This extra computation is performed only at the initial iteration and in our experience change in diagonal of M is insignificant (less than 0.01%) with the iterations. So λ_i is obtained at the initial iteration is used in subsequent iterations.

The parameter (model) resolution using the three penalties discussed in this work showed that the model-resolution based penalty provides optimal resolution characteristics and the same is evident from Fig. 2. It is interesting to note that the standard (constant) penalty term resulted in resolution characteristics following the similar trend of sensitivity plots observed in [23], showing that the parameter resolution is more biased toward the edge. The improvement in the resolution is more evident at the center of imaging domain (comparing value of 0.25 for model-resolution based regularization with 0.01 using other penalty terms). The same is also proven using numerical experiments, where the resolution of two targets that are placed close together is taken up as a test case (Fig. 4). Note that the same trend has not been observed in 3D (Fig. 6). Even though spatially varying regularizations provided better resolution, the improvement between exponential penalty and model-resolution penalty is not significant [Fig. 6(b)]. This is primarily because the sensitivity of 3D imaging is at least 5 orders of magnitude less compared to 2D [23–24], resulting in poor resolution characteristics.

The free regularization parameters and weights used in this work are kept constant for all numerical examples discussed, and these were chosen based on the prior experience of authors. Any deviations from this choice lead to deterioration of the reconstructed image quality or lead to meaningless results. Also, when the distance between the targets (having radius of 5 mm or more) either in 2D or 3D has been decreased less than 5 mm (which is the typical resolution of diffuse optical imaging), all regularization schemes discussed here failed to resolve these targets (not shown here). Also when the target size is below 5 mm, the same trend is observed. This asserts that no penalty term cannot overcome the inherent resolution limitation of diffuse imaging. The new regularization scheme can only improve the qualitative (resolution) and quantitative nature of the reconstructed images compared to the traditional ones, provided there is enough sensitivity of the imaging problem. It might be also the case where the penalty term is dominating the optimization scheme resulting in highly smooth image.

The data importance using data-resolution characteristics (Fig. 3) for three-regularization schemes also showed similar characteristics as model-resolution matrix (Fig. 2). The model-resolution based penalty fairs better compared to

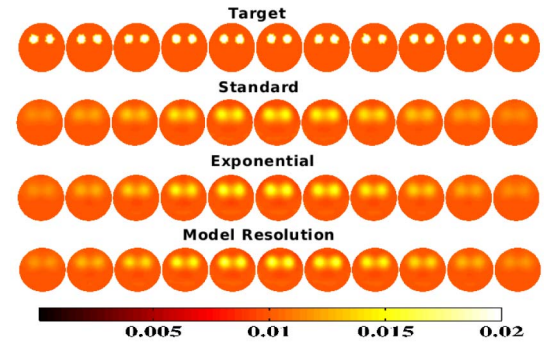

(a)

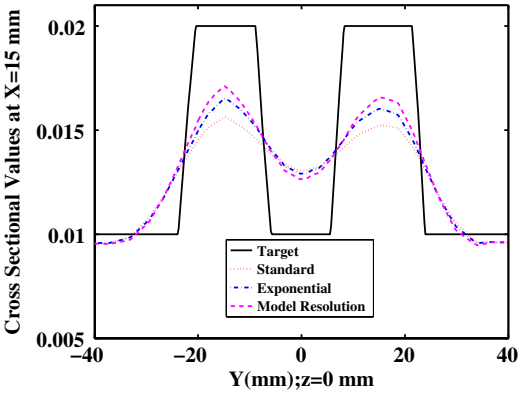

(b)

Fig. 7. (Color online) Similar effort to Fig. 6 with targets located close to the boundary (edge) of the imaging domain.

exponential penalty and standard penalty taking the lowest value, meaning that the importance of data points is greater when model-resolution penalty is used and results in better usage of acquired data, leading to better quality of reconstructed images.

Even though this work is focused more on diffuse optical imaging, the developed methodology could be used for other imaging modalities whose imaging principles are similar to diffuse optical imaging, examples being fluorescence optical tomography [25], bioluminescence tomography [26], electrical impedance tomography [27], and electrical capacitance tomography [28]. Also, the imaging domains that are considered are regularly shaped, but the observed trends and conclusions of this work should hold good for irregular shaped real tissues as well.

This work introduced a new penalty/regularization scheme based on the model of the problem and also provided a quantitative way of assessing the performance characteristics of the regularization schemes using both model-resolution and data-resolution matrices. Note that assessing these characteristics does not require performing the image reconstruction procedure and also does not depend on the data (or noise in it). The regularization scheme based on model-resolution provided better performance characteristics compared to others.

5. CONCLUSIONS

As regularization/penalty scheme plays an important role in obtaining good quality reconstructed optical images in diffuse optical tomography, this work presented a regularization scheme based on the model of the problem, called as model-resolution based penalty. The motivation for this arises from spatially varying regularization introduced earlier by Pogue *et. al* [10], and a formal approach for obtaining the regularization has been presented. Also objectively evaluating the new regularization scheme (or any regularization) using the model and data-resolution characteristics was also presented along with numerical evidence backing up observed trends. The model-resolution based regularization scheme was shown to provide better optical images both qualitatively and quantitatively. This asserts that model-resolution based regularization holds a promise to become the mainstream regularization scheme in diffuse optical tomography. The experimental verification of the trends observed in this work is being pursued as a future work.

ACKNOWLEDGMENTS

This work was supported by the Department of Atomic Energy Young Scientist Research Award (No. 2010/20/34/6/BRNS) by the government of India. P.K.Y. acknowledges the Apple Lauerate award.

REFERENCES

1. D. A. Boas, D. H. Brooks, E. L. Miller, C. A. DiMarzio, M. Kilmer, R. J. Gaudette, and Q. Zhang, "Imaging the body with diffuse optical tomography," IEEE Signal Process. Mag. **18**, 57–75 (2001).
2. S. L. Jacques and B. W. Pogue, "Tutorial on diffuse light transport," J. Biomed. Opt. **13**, 041302 (2008).
3. A. Gibson, J. C. Hebden, and S. R. Arridge, "Recent advances in diffuse optical tomography," Phys. Med. Biol. **50**, R1–R43 (2005).
4. A. Gibson and H. Dehghani, "Diffuse optical imaging," Phil. Trans. R. Soc. A **367**, 3055–3072 (2009).
5. S. R. Arridge, "Optical tomography in medical imaging," Inverse Probl. **15**, R41–R93 (1999).
6. S. R. Arridge and J. C. Hebden, "Optical imaging in medicine: II. Modelling and reconstruction," Phys. Med. Biol. **42**, 841–853 (1997).
7. H. Dehghani, S. Srinivasan, B. W. Pogue, and A. Gibson, "Numerical modelling and image reconstruction in diffuse optical tomography," Phil. Trans. R. Soc. A **367**, 3073–3093 (2009).
8. X. Intes, C. Maloux, M. Guven, B. Yazici, and B. Chance, "Diffuse optical tomography with physiological and spatial a priori constraints," Phys. Med. Biol. **49**, N155–N163 (2004).
9. M. Guven, B. Yazici, X. Intes, and B. Chance, "Diffuse optical tomography with a priori anatomical information," Phys. Med. Biol. **50**, 2837–2858 (2005).
10. B. W. Pogue, T. McBride, J. Prewitt, U. L. Osterberg, and K. D. Paulsen, "Spatially variant regularization improves diffuse optical tomography," Appl. Opt. **38**, 2950–2961 (1999).
11. H. Niu, P. Guo, L. Ji, Q. Zhao, and T. Jiang, "Improving image quality of diffuse optical tomography with a projection-error-based adaptive regularization method," Opt. Express **16**, 12423–12434 (2008).
12. N. Cao, A. Nehorai, and M. Jacob, "Image reconstruction for diffuse optical tomography using sparsity regularization and expectation-maximization algorithm," Opt. Express **15**, 13695–13708 (2007).
13. P. K. Yalavarthy, B. W. Pogue, H. Dehghani, and K. D. Paulsen, "Weight-matrix structured regularization provides optimal generalized least-squares estimate in diffuse optical tomography," Med. Phys. **34**, 2085–2098 (2007).
14. P. K. Yalavarthy, B. W. Pogue, H. Dehghani, C. M. Carpenter, S. Jiang, and K. D. Paulsen, "Structural information within regularization matrices improves near infrared diffuse optical tomography," Opt. Express **15**, 8043–8058 (2007).
15. M. E. Eames and H. Dehghani, "Wavelength dependence of sensitivity in spectral diffuse optical imaging: effect of normal-

ization on image reconstruction," Opt. Express **16**, 17780–17791 (2008).
16. F. Larusson, S. Fantini, and E. L. Miller, "Hyperspectral image reconstruction for diffuse optical tomography," Biomed. Opt. Express **2**, 946–965 (2011).
17. S. R. Arridge and M. Schweiger, "Photon-measurement density functions. Part 2: Finite-element-method calculations," Appl. Opt. **34**, 8026–8037 (1995).
18. M. Schweiger, S. R. Arridge, M. Hiroaka, and D. T. Delpy, "The finite element model for the propagation of light in scattering media: Boundary and source conditions," Med. Phys. **22**, 1779–1792 (1995).
19. M. Schweiger, S. R. Arridge, and I. Nissila, "Gauss-Newton method for image reconstruction in diffuse optical tomography," Phys. Med. Biol. **50**, 2365–2386 (2005).
20. M. S. Zhdanov, *Geophysical Inverse Theory and Regularization Problems* 1st ed. (Elsevier Science, 2002).
21. T. O. Mcbride, B. W. Pogue, S. Jiang, U. L. Osterberg, and K. D. Paulsen, "A parallel-detection frequency-domain near-infrared tomography system for hemoglobin imaging of the breast in vivo," Rev. Sci. Instrum. **72**, 1817–1824 (2001).
22. H. Dehghani, M. E. Eames, P. K. Yalavarthy, S. C. Davis, S. Srinivasan, C. M. Carpenter, B. W. Pogue, and K. D. Paulsen, "Near infrared optical tomography using NIRFAST: Algorithms for numerical model and image reconstruction algorithms," Commun. Numer. Methods Eng. **25**, 711–732 (2009).
23. P. K. Yalavarthy, H. Dehghani, B. W. Pogue, and K. D. Paulsen, "Critical computational aspects of near infrared circular tomographic imaging: Analysis of measurement number, mesh resolution and reconstruction basis," Opt. Express **14**, 6113–6127 (2006).
24. M. Schweiger and S. R. Arridge, "Comparison of two- and three-dimensional reconstruction methods in optical tomography," Appl. Opt. **37**, 7419–7428 (1998).
25. S. C. Davis, H. Dehghani, J. Wang, S. Jiang, B. W. Pogue, and K. D. Paulsen, "Image-guided diffuse optical fluorescence tomography implemented with Laplacian-type regularization," Opt. Express **15**, 4066–4082, (2007).
26. S. Ahn, A. J. Chaudhari, F. Darvas, C. A. Bouman, and R. M. Leahy, "Fast iterative image reconstruction methods for fully 3D multispectral bioluminescence tomography," Phys. Med. Biol. **53**, 3921–3942 (2008).
27. L. Borcea, "Electrical impedance tomography," Inverse Probl. **18**, R99–R136 (2002).
28. M. Soleimani, P. K. Yalavarthy, and H. Dehghani, "Helmholtz-type regularization method for permittivity reconstruction using experimental phantom data of electrical capacitance tomography," IEEE Trans. Instrum. Meas. **59**, 78–83 (2010).